

Correlations Between Planetary Microlensing Parameters

Cheongho Han, Kyu-Ha Hwang, and Yoon-Hyun Ryu

*Department of Physics, Chungbuk National University, Cheongju 361-763,
Republic of Korea; cheongho,kyuha,yhryu@astroph.chungbuk.ac.kr*

ABSTRACT

Characterization of microlensing planets requires modeling of observed light curves including many parameters. Studying the dependency of the pattern of light curves on the lensing parameters and the correlations between the parameters is important to understand how the uncertainties of the planetary parameters are propagated from other parameters. In this paper, we show that despite the apparent complexity of the pattern of light curves of planetary lensing events, the correlations between the lensing parameters can be understood by studying how the parameters affect the characteristics of lensing light curves such as the height and width, the caustic-crossing time scale, and the location and duration of planetary perturbations. Based on analytic arguments about the dependency of light curve features on the parameters, we obtain the correlations for the two representative cases of planetary events. We also demonstrate the applicability of the correlations to general planetary events by actually obtaining the correlations from modelings of light curves produced by simulations.

Subject headings: gravitational lensing

1. Introduction

A microlensing event occurs when an astronomical object (lens) is closely aligned with the line of sight toward a background star (source). Microlensing causes change of the source star brightness and the resulting light curve is characterized by its smooth variation (Paczynski 1986). If the lensing object is a star and it contains a planet, the resulting light curve can exhibit a discontinuous signature of the planet on the smooth light curve of the primary-induced event, and thus microlensing can be used as a method to search for extrasolar planets (Mao, & Paczynski 1991; Gould & Loeb 1992). Microlensing is sensitive to planets that are generally inaccessible to other methods, in particular cool planets at or beyond the snow line, very low-mass planets, planets orbiting low-mass stars, free-floating

planets, and even planets in external galaxies. Therefore, when combined with the results from other surveys, microlensing planet searches can yield an accurate and complete census of the frequency and properties of planets. Since the first discovery in 2004, 9 microlensing planets have been reported (Bond et al. 2004; Udalski et al. 2005; Beaulieu et al. 2006; Gould et al. 2006; Gaudi et al. 2008; Bennett et al. 2008; Dong et al. 2009; Sumi et al. 2010; Janczak et al. 2010).

Characterization of microlensing planets requires modeling of observed light curves. This modeling process requires to include many parameters because the pattern of lensing light curves and the signals of planets take different forms depending on the combination of these parameters. Therefore, studying the dependency of the pattern of light curves on the lensing parameters and the correlations between the parameters help to understand how the uncertainties of the planetary parameters are propagated from other lensing parameters. This also helps to establish observational strategies for better characterization of planets. However, it appears that the correlations between the lensing parameters are very complex due to the enormous diversity of lensing light curves resulting from the combinations of the numerous parameters.

In this paper, we show that despite the apparent complexity of the pattern of light curves of planetary lensing events, the correlations between the lensing parameters can be understood based on the dependency of the characteristic features of lensing light curves on the parameters. We provide the correlations for the two representative cases of planetary events. We also demonstrate the applicability of the correlations to general planetary lensing events by actually obtaining the correlations from modelings of light curves produced by simulations.

2. Parameters

The microlensing signal of a planet is a brief perturbation to the smooth standard light curve of the primary-induced single-lensing event. Therefore, the parameters needed to describe planetary lensing light curves are broadly divided into two categories. The first set of parameters is needed to describe the light curve of a standard single-lens event produced by the star hosting the planet. These parameters include the closest lens-source separation normalized by the Einstein radius, β (impact parameter), the time of the closest lens-source approach, t_0 , the time required for the source to transit the Einstein radius of the lens, t_E (Einstein time scale), the flux from the lensed star, F_S , and the blended flux, F_B . With these parameters, the single-lensing light curve is represented by

$$F(t) = F_S A(t) + F_B, \tag{1}$$

where

$$A(u) = \frac{u^2 + 2}{u(u^2 + 4)^{1/2}}; \quad u(t) = \left[\left(\frac{t - t_0}{t_E} \right)^2 + \beta^2 \right]^{1/2}. \quad (2)$$

Here u represents the lens-source separation normalized by the Einstein radius θ_E . These parameters characterize the global shape of lensing light curves such as the height and width.

Besides the single-lensing parameters, additional parameters are needed to describe the detailed structure of the perturbations induced by planets. These parameters include the planet/star mass ratio, q , the projected star-planet separation normalized by the Einstein radius, s , and the angle between the source trajectory and the star-planet axis, α . Since planetary perturbations are produced in most cases by close approaches or crosses of source stars over caustics, an additional parameter of the source size normalized by the Einstein radius, ρ_* , is needed to describe the deviation of the perturbation affected by the finite-source effect. From the combinations of the lensing parameters, the light curves of planetary events exhibit various patterns.

3. Correlations

3.1. Single-Lensing Parameters

The correlations between the single-lensing parameters can be found by investigating how the global features of lensing light curves such as the height and width vary depending on the parameters. The height of the light curve is determined by the combination of the impact parameter β and the blended light ratio, $f_B = F_B/F_S$. When affected by blended flux, the impact parameter estimated based on the apparent height of the light curve is related to the blended light ratio as

$$\beta_B = [2(1 - A_{\max,B}^{-2})^{-1/2} - 2]^{1/2}; \quad A_{\max,B} = \frac{A_{\max} + f_B}{1 + f_B}, \quad (3)$$

where $A_{\max,B}$ is the apparent peak magnification. Then, with the increase of f_B , $A_{\max,B}$ decreases, and thus β_B increases, implying that as the blended light increases, the peak magnification appears to be lower, and the resulting impact parameter becomes larger. Therefore, it is found that *the blended flux ratio f_B and the impact parameter β are correlated*.

Blending affects not only the height but also the width of light curves. The event time scale estimated from the width of the blended light curve, $t_{E,B}$, differs from the true value,

t_E . The relation between the two time scales is (Han 1999)

$$t_{E,B} = t_E \left(\frac{\beta_{\text{th},B}^2 - \beta^2}{\beta_{\text{th}}^2 - \beta_B^2} \right)^{1/2}. \quad (4)$$

Here $\beta_{\text{th},B}$ and β_{th} represent the threshold impact parameters of the source trajectory for event detections with the presence and absence of blended flux, respectively. Because of blending, the threshold magnification is increased by $A_{\text{th},B} = A_{\text{th}}(1 + f_B) - f_B$ and thus the corresponding threshold impact parameter is lowered by $\beta_{\text{th},B} = [2(1 - A_{\text{th},B}^{-2})^{-1/2} - 2]^{1/2}$, implying that to be detected the source star of a blended event should approach the lens closer than an unblended event. From equation (4), it is found that the increase of blended flux causes the measured event time scale shorter. Therefore, *the blended flux ratio f_B and the Einstein time scale t_E are anti-correlated*. Since the blended flux ratio is correlated with the impact parameter, while it is anti-correlated with the time scale, it is found that *the impact parameter β and the time scale t_E are anti-correlated*.

3.2. Binary Parameters

The major constraint on the the normalized planetary separation s comes from the location of the planetary perturbation on the light curve. This is because the location of the caustic with respect to the primary lens, \mathbf{u}_p , is related to the position vector to the planet from the primary, \mathbf{s} , by (Griest & Safizadeh 1998)

$$\mathbf{u}_p = \mathbf{s} - \frac{1}{s}. \quad (5)$$

The primary-caustic separation, u_p , varies differently depending on whether the planet is inside ($s < 1$) or outside ($s > 1$) of the Einstein radius. For planets with $s > 1$, the caustic separation u_p increases with the increase of the planetary separation s . By contrast, the caustic separation decreases as the planet separation increases. In addition, the type of the perturbation differs depending on the location of the planet. When the planet is located outside the Einstein ring ($s > 1$), it perturbs the major image among the two images produced by the primary lens (Gaudi & Gould 1997), resulting in higher magnifications than those of the adjacent part of the single-lensing light curve during the perturbation. When the planet is inside the Einstein ring ($s < 1$), by contrast, it perturbs the minor image and the magnifications during the perturbation are lower than those of the single-lensing light curve. From the relation in equation (5) combined with the geometry of the lens system presented in Figure 1, it is found that the relative location of the perturbation on the light curve is related to the time of perturbations, t_p , and other lensing parameters by

$$\frac{t_p - t_0}{t_E} = (u_p^2 - \beta^2)^{1/2}. \quad (6)$$

Then, for planets with $s > 1$, as s increases, u_p increases, and thus the impact parameter β should increase to match the constraint given by the location of the perturbation on the observed light curve. For planets with $s < 1$, by contrast, u_p decreases with the increase of s , and thus β decreases. Therefore, it is found that *the planetary separation s and the impact parameter β are correlated for planetary events with major-image perturbations ($s > 1$) and anti-correlated for events with minor-image perturbations ($s < 1$).*

The correlation between the planetary separation s and the mass ratio q is mainly given by the duration of the planetary perturbation. The duration is proportional to the size of the caustic. The size of the caustic as measured by the width along the primary-planet axis is related to s and q (Han 2006) by

$$w_c = \begin{cases} 4q^{1/2}/[s^2(1 - s^{-2})] & \text{for } s > 1, \\ 2q^{1/2}(\kappa - \kappa^{-1} + \kappa s^{-2}) & \text{for } s < 1, \end{cases} \quad (7)$$

where $\kappa^2 = [\cos 2\theta \pm (s^4 - \sin^2 2\theta)^{1/2}]/(s^2 - s^{-2})$ and $\theta = \pi/2 \pm \sin^{-1}(\sqrt{3}s^2/2)/2$. In the limiting cases of planetary separations of $s \gg 1$ and $s \ll 1$, the relations are expressed in compact forms of

$$w_c = \begin{cases} 4q^{1/2}s^{-2} & \text{for } s \gg 1, \\ 3\sqrt{3}q^{1/2}s^3/4 & \text{for } s \ll 1, \end{cases} \quad (8)$$

respectively. Then, from the relation between s and q combined with the constraint of the perturbation duration measured from the light curve, it is found that *the planetary separation and the mass ratio should be correlated for planetary events with major-images perturbations ($s > 1$) and anti-correlated for events with minor-image perturbations ($s < 1$).*

The main constraint on the normalized source radius ρ_\star is provided by the duration of caustic-crossings (caustic-crossing time scale). The caustic-crossing time scale is related to the normalized source radius ρ_\star and the Einstein time scale t_E by

$$\Delta t_{cc} = \frac{\rho_\star}{\sin \psi} t_E, \quad (9)$$

where ψ represents the angle between the caustic and the source trajectory. Then, to match the constraint of the caustic-crossing time scale measured from the observed light curve, *the normalized source radius ρ_\star and the Einstein time scale t_E should be anti-correlated.*

In Table 1, we summarize the correlations between the lensing parameters. Here, the correlations between the pairs of parameters not mentioned in the text are deduced from the correlations with other parameters. For example, we deduce the correlation between the normalized source radius ρ_\star and the impact parameter β based on the correlations between ρ_\star - t_E and t_E - β parameter pairs. In the table, we mark “↗” for the pairs of parameters that

are correlated, while the correlation is marked by “ \searrow ” for the pairs of parameters that are anti-correlated.

Gould & Welch (1996) studied the relation between the normalized source radius and the impact parameter for high-magnification single-lens events. See also Gaudi & Gould (1997) for the relation between the lens-source proper motion, μ , and the time scale, although μ is not a standard planetary lensing parameter.

4. Demonstration

In the previous section, we investigated the correlations between the lensing parameters based on analytic arguments about the dependency of the characteristic features of lensing light curves on the parameters. In this section, we demonstrate that the correlations are applicable to general planetary microlensing events by actually obtaining the correlations from modelings of light curves produced by simulations.

We produce two light curves of planetary lensing events, where the individual curves represent those of events with major and minor-image perturbations, respectively. The light curves are produced considering the strategy of the current planetary lensing experiments where events are detected through modest-cadence survey observations and perturbations are densely covered by follow-up observations. We set the photometric uncertainty by assuming that the photometry follows photon statistics with a 1% systematic uncertainty and the deviations of the data points are Gaussian distributed. The other factors affecting the photometry such as the source brightness and blending are based on the values of typical Galactic bulge events. Figure 2 shows the light curves of the events produced by the simulation where the upper and lower panels are those of the events with major and minor-image perturbations, respectively. The inset in each panel shows the geometry of the event where the straight line with an arrow is the source trajectory and the temperature scale represents magnifications where a brighter tone implies a higher magnification.

We search for the solution of the lensing parameters by conducting modeling of the simulated light curves. In modeling planetary lensing light curves, it is difficult to conduct brute-force search throughout all parameter space due to the large number of parameters. In addition, it is difficult to conduct simple downhill approach due to the complexity of the χ^2 surface. We, therefore, use a hybrid approach where grid searches are conducted over the space of parameters of s , q , and α and the remaining parameters are allowed to vary so that the model light curve results in minimum χ^2 at each grid point. We use a Markov Chain Monte Carlo method for χ^2 minimization. Once the solutions of the individual grid

points are determined, the best-fit model is obtained by comparing the χ^2 minima of the individual grid points. The uncertainties of the best-fit parameters are estimated based on the chains of solutions produced by modeling. For the computations of lensing magnifications including finite-source effect, we use the ray-shooting method where a large number of rays are shot from the image plane, bent according to the lens equation, and arrive on the source plane. Then, the magnification corresponding to the location of a source star is computed by comparing the number density of rays on the source star with the density on the image plane. We minimize the computation time by restricting the region of ray shooting around the images and thus minimizing the number of rays needed for the computations of finite-source magnifications. We also apply semi-analytic hexadecapole approximation (Pejcha & Heyrovský 2009; Gould 2008) for magnification computations in the region where the effect of source size is not important.

In Figure 3 and 4, we present the results of the modeling for the planetary events with major and minor image perturbations, respectively. The individual panels of each figure show the contour plots of χ^2 in the spaces of the combinations of the lensing parameters. To directly compare the correlations, we arrange the panels according to the same order of the parameters presented in Table 1. From the comparison, it is found that the correlations found from modeling coincide with those predicted based on analytic arguments. This implies that the correlations presented in Table 1 are applicable to general planetary microlensing events.

5. Conclusion and Discussion

We investigated the correlations between the parameters of planetary lensing events. From this, we found that the correlations could be understood by studying how the lensing parameters affect the characteristics of lensing light curves such as the height and width of the light curve, the caustic-crossing time scale, and the location and duration of perturbations. Based on analytic arguments about the dependency of the features of lensing light curves on the parameters, we obtain the correlations. We also demonstrated the applicability of the correlations to general planetary lensing events by actually obtaining the correlations from modelings of light curves produced by simulations.

Understanding the correlations between lensing parameters can help to setup observational strategies for better constraints of the planetary parameters. For example, the correlations between the blending and planetary parameters imply that blending affects determinations of the planetary parameters and thus de-blending or precise determination of the blending parameter is important to better constrain the planetary parameters. Several methods can be applied to resolve the blending problem. Photometrically, it is known that

good coverage of the peak region and wings of light curves by follow-up observations help to constrain the blending parameter (Thomas & Griest 2006). High resolution imaging from space observations (Han 1997) or ground-based AO imaging (Bennett et al. 2010) can help to resolve source stars from blended stars. Astrometric measurement of the blended image centroid can also help to identify the lensed source among blended stars (Alard et al. 1995). Precise and dense coverage of the perturbation is another way to constrain the planet parameters. This is because not only the location of perturbations but also their shape provides constraints on planetary parameters.¹ Then, even if the location of the perturbation is uncertain due to severe blending, it is still possible to constrain the planetary parameters from the shape of the perturbation.

This work is supported by Creative Research Initiative program (2009-0081561) of National research Foundation of Korea.

REFERENCES

- Alard, C., Mao, S., & Guibert, J. 1995, *A&A*, 300, L17
- Beaulieu, J. P., et al. 2006, *Nature*, 439, 437
- Bennett, D. P., et al. 2008, *ApJ*, 684, 663
- Bennett D. P., et al. 2010, *ApJ*, 713, 837
- Bond, I. A., et al. 2004, *ApJ*, 606, L155
- Dong, S., et al., 2009, *ApJ*, 698, 1826
- Gaudi, B. S., & Gould, A. 1997, *ApJ*, 486, 85
- Gaudi, B. S., et al. 2008, *Science*, 319, 927
- Gould, A. 2008, *ApJ*, 681, 1593

¹The shape of perturbations is basically determined by the caustic shape, which depends on the planetary separation. Therefore, precise and dense coverage of perturbations is another way to improve the precision of planetary parameter measurements. This is the same reason why it is possible to constrain the planetary parameters from the analysis of planetary perturbations occurring on high-magnification events. These perturbations occur near the peak of light curves regardless of the planetary separation. Nevertheless, it is possible to constrain the planetary parameters by analyzing the shape of perturbations.

- Gould, A., & Loeb, A. 1992, ApJ, 396, 104
- Gould, A., & Welch, D. L. 1996, ApJ, 464, 212
- Gould, A., et al. 2006, ApJ, 644, L37
- Griest, K., & Safizadeh, N. 1998, ApJ, 500, 37
- Han, C. 1997, ApJ, 490, 51
- Han, C. 1999, MNRAS, 309, 373
- Han, C. 2006, ApJ, 638, 1080
- Janczak, J., et al. 2010, ApJ, 711, 731
- Mao, S., & Paczynski, B. 1991, ApJ, 374, L37
- Paczynski, B. 1986, ApJ, 304, 1
- Pejcha, O., & Heyrovský, B. 2009, ApJ, 690, 1772
- Sumi, T., et al. 2010, ApJ, 710, 1641
- Thomas, C. L., & Griest, K. 2006, ApJ, 640, 299
- Udalski, A., et al. 2005, ApJ, 628, L109

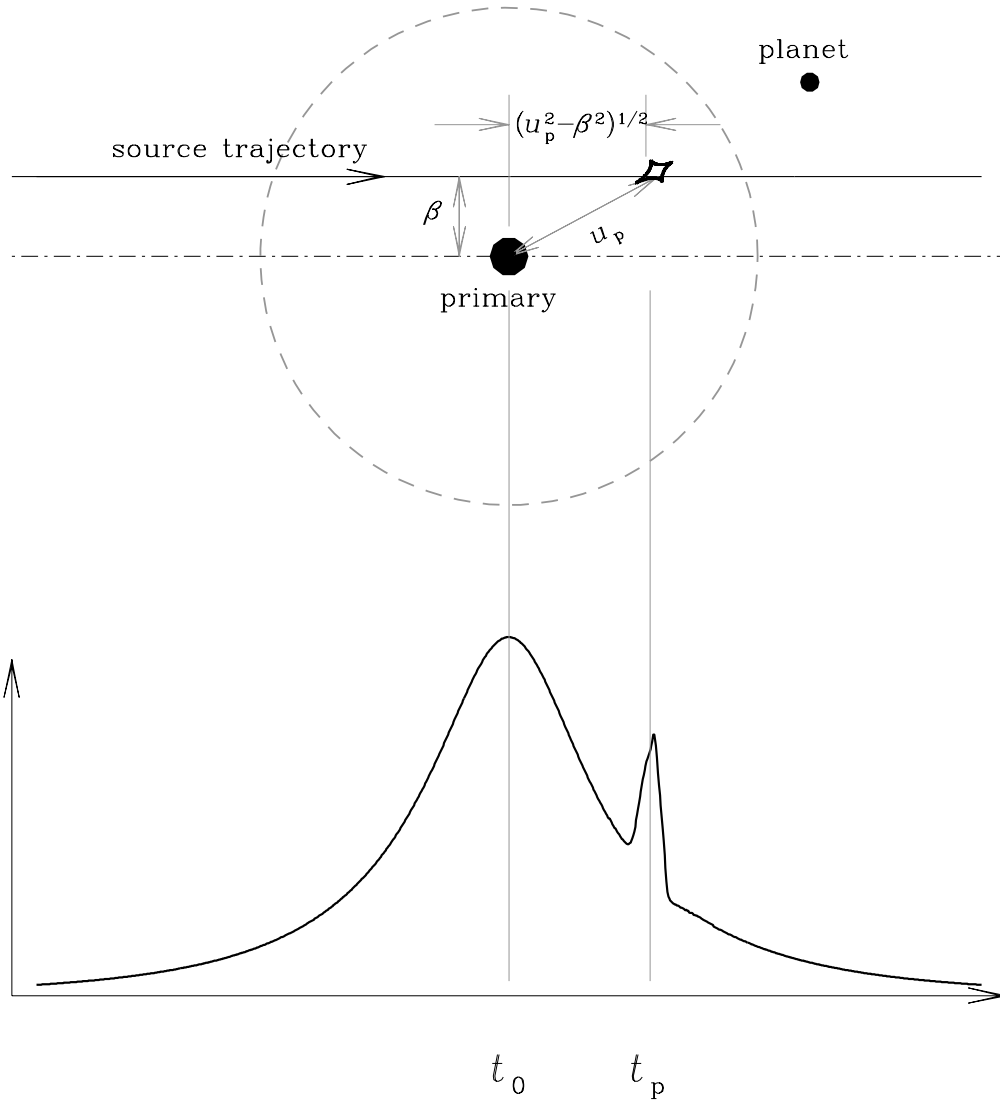


Fig. 1.— The geometry of the lens system showing the relation between the location of the planetary perturbation and lensing parameters. The large dashed circle represents the Einstein ring and the small closed figure connected by concave curves is the caustic induced by the planet.

Table 1. Correlations Between Lensing Parameters

	β	t_E	ρ_*	$s (s > 1)$	$q (s > 1)$	$s (s < 1)$	$q (s < 1)$
β	\nearrow						
t_E	\searrow	\nearrow					
ρ_*	\nearrow	\searrow	\nearrow				
$s (s > 1)$	\nearrow	\searrow	\nearrow	\nearrow			
$q (s > 1)$	\nearrow	\searrow	\nearrow	\nearrow	\nearrow		
$s (s < 1)$	\searrow	\nearrow	\searrow			\nearrow	
$q (s < 1)$	\nearrow	\searrow	\nearrow			\searrow	\nearrow

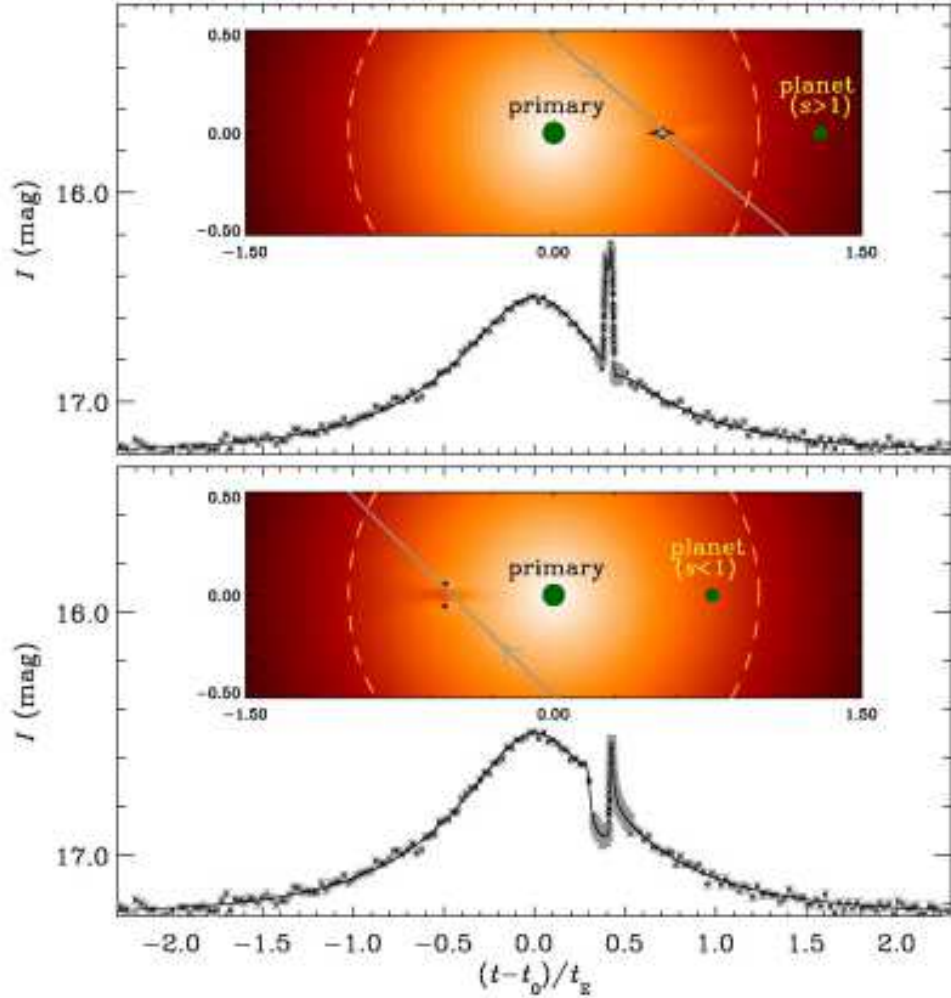


Fig. 2.— Light curves of planetary lensing events with major (upper panel) and minor-image (lower panel) perturbations. The inset in each panel shows the geometry of the event where the locations of the primary and planet, source trajectory (straight line with an arrow), caustic (small closed figure), and Einstein ring (big dashed circle) are marked. The correlations between the lensing parameters of the individual events are presented in Fig. 3 and 4, respectively.

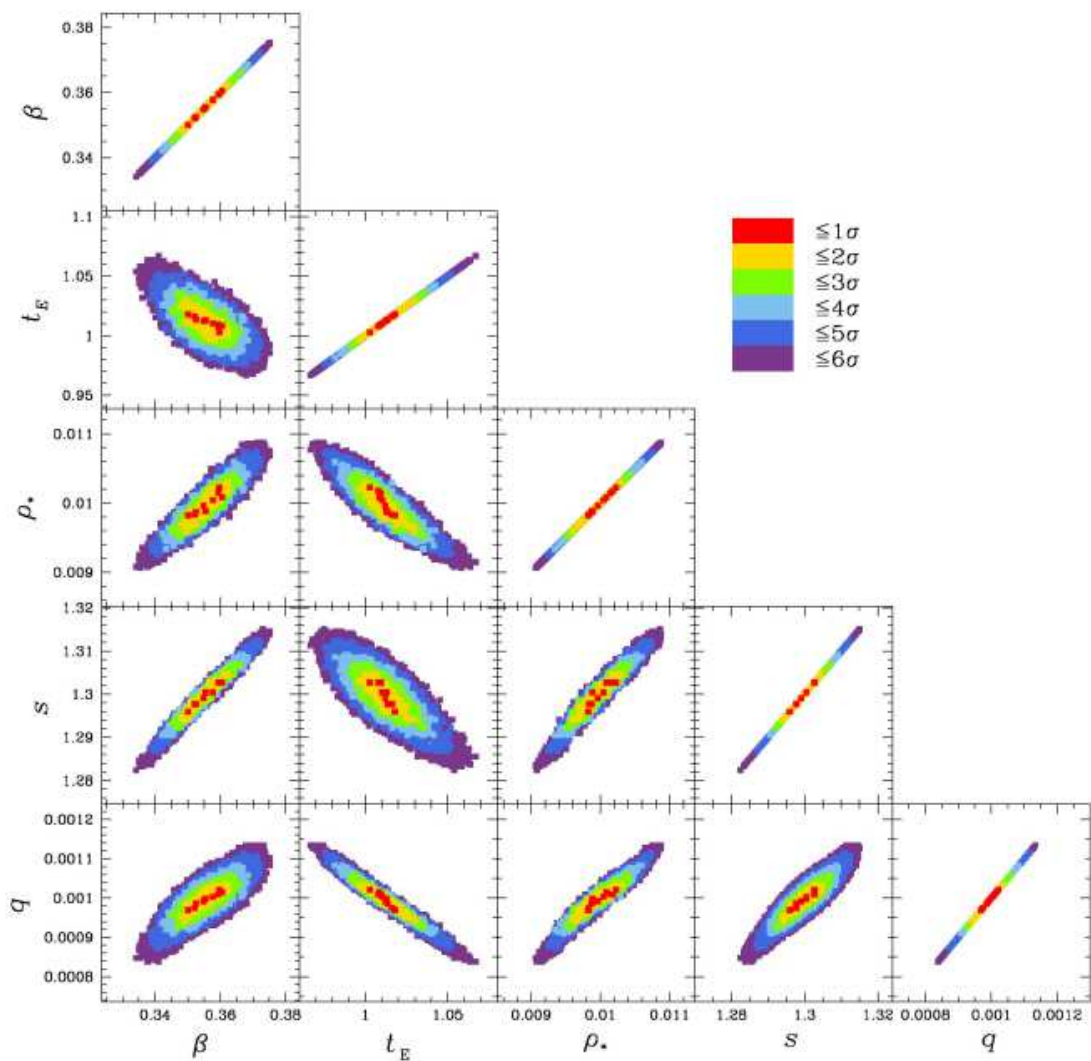


Fig. 3.— Contours of χ^2 in the spaces of various combinations of lensing parameters for the planetary event with a major-image perturbations. The result is based on the modeling of the light curve presented in the upper panel of Fig. 2. For direct comparison of the correlations to those presented in Table 1, the order of parameters are arranged accordingly.

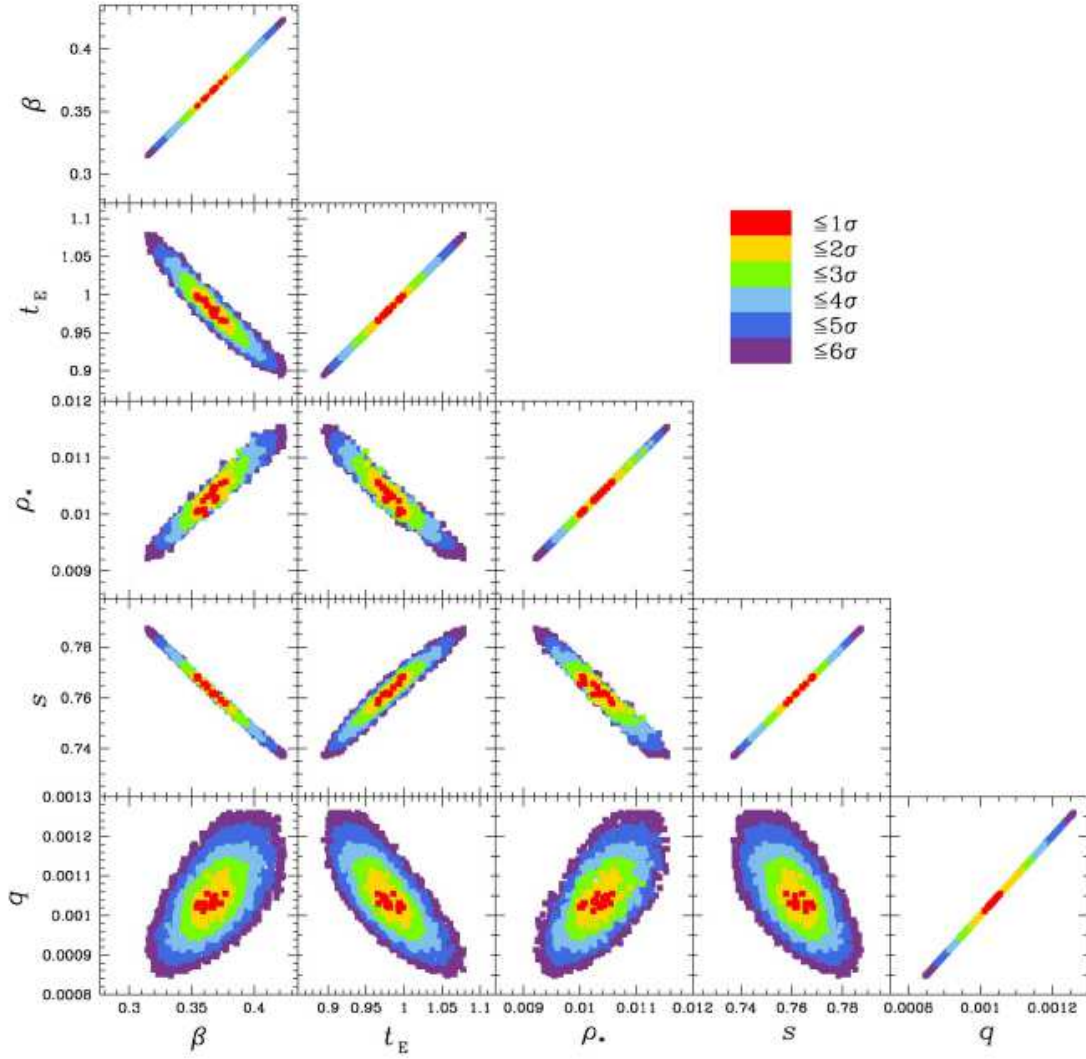


Fig. 4.— Same as in Fig. 3 except that the correlations are for the planetary event with a minor-image perturbation.